

## Atomic motion in hollow submicron circular cylinders

S. Al-Awfi and M. Babiker

*Department of Physics, University of Essex, Colchester, Essex CO4 3SQ, England*

(Received 24 August 1999; published 10 February 2000)

The motion of atoms inside a long hollow cylindrical waveguide with a circular cross section is investigated. The guide is assumed to have subwavelength dimensions, in which case the spontaneous decay process is effected only by emission of a few possible cavity modes. The characteristics of the atomic motion in the guide are explored in the presence of an excited waveguide mode. We show that the atomic motion in this case is determined by an axial channelling force and a trapping dipole force, plus a quantized light torque associated with the orbital angular momentum property of excited waveguide modes of order  $\ell > 0$ . It is predicted that in addition to its axial motion, an atom subject to such a mode should be trapped radially in a vibrational state and should exhibit interesting rotational features due to the light torque, including a rotational frequency shift.

PACS number(s): 42.50.Vk, 32.70.Jz, 32.80.Pj, 32.80.Lg

### I. INTRODUCTION

In our previous papers [1,2] we were concerned with the theory of atomic motion in spatially varying light fields inside two types of waveguide: the parallel plate guide and the cylindrical guide with rectangular cross section. This paper is devoted to the case of cylindrical waveguides with a circular cross section which are more common in practice (for example in fibre optics [3]). We are also interested in this type of cross section because, first, it is currently receiving attention in the context of cavity QED, including recent work by Rippin and Knight, Kakazu, and Kim and by Nha and Jhe [4] and secondly, the structure is important for guiding atoms [5–11].

In addition to the new geometry which is known to modify spontaneous emission [4], we expect consequent modifications of atom dynamics relative to the cases in Refs. [1,2]. The focus of the paper is thus on the atom dynamics in the subwavelength regime. We show here that the circular guide gives rise to additional effects in atom dynamics which could not have been realized in Refs. [1,2]. These are due to the orbital angular momentum property associated with the azimuthal dependence of the circular cylinder field structure. The interaction of the atom with a waveguide mode of order greater than the fundamental mode gives rise to a number of rotational effects which make the atomic motion drastically different from that associated with the fundamental mode of the waveguide. The characteristics of the atomic motion in the guide are then explored for an electric dipole within the guide subject to an excited  $p$ -polarized mode. We also consider the rotational features including a rotational shift due to the azimuthal dependence of the field structure which arises in the interaction of the atom with any waveguide mode of order  $\ell > 0$ .

The paper is organized as follows. In Sec. II we outline the procedure leading to quantized electromagnetic modes inside a circular waveguide. This readily facilitates the evaluation of the spontaneous emission rate for an electric dipole within the circular guide and the variation of this rate with the radius of the cross section. The subwavelength regime is emphasized where only a few modes are responsible for the spontaneous emission. In Sec. III we illustrate the

results by considering the case of sodium atoms in subwavelength waveguides. In Sec. IV we consider the kinematics of such atoms within the guide and in Sec. V we discuss the dynamical effects on the motion when a cavity mode is excited. Section VI contains comments and conclusions.

### II. QED IN WAVEGUIDE

The hollow cylindrical waveguide with circular cross section is depicted in Fig. 1. As shown in this figure,  $a$  is the radius, the waveguide is infinite in length and the longitudinal spatial variation is along the  $z$  axis, coincident with the straight line  $r=0$ . The walls of the structure are perfectly conducting excluding all electromagnetic fields from their interior. The standard electromagnetic boundary conditions apply such that the tangential components of the electric field vector and the magnetic field vector must vanish at every point on the cylinder surface.

The system consists of an atom of mass  $M$ , characterized by its electric dipole moment  $\mathbf{d}$ , of oscillation frequency  $\omega_0$ , interacting with the electromagnetic field. The effective Hamiltonian can be written as

$$H = \frac{p^2}{2M} + U(\mathbf{R}) + \hbar \omega_0 \pi^+ \pi - \mathbf{d} \cdot \mathbf{E}(\mathbf{R}) + H_{\text{field}} \quad (1)$$

where  $\mathbf{P}$  and  $\mathbf{R}$  are the momentum and position vectors of the atomic center of mass which is assumed to be subject to a general potential  $U(\mathbf{R})$ . In the two-level approximation, the internal motion of the atom involves only two states  $|e\rangle$ , of energy  $E_e$ , and  $|g\rangle$ , of energy  $E_g$ , such that  $E_e - E_g = \hbar \omega_0$ . The operators  $\pi$  and  $\pi^+$  are the lowering and raising



FIG. 1. Schematic drawing of the hollow circular waveguide of infinite length. The cylinder wall is assumed to be perfectly conducting.

operators for the internal atomic states such that  $\mathbf{d} = \langle \mathbf{d} \rangle_{eg}(\pi + \pi^\dagger)$ ;  $\mathbf{E}$  is the electric field operator and  $H_{\text{field}}$  is the electromagnetic field Hamiltonian.

### A. Quantized fields

The procedure for enumerating the electromagnetic modes inside the cylinder begins with the solution of the wave equation for the transverse electromagnetic fields. As is well known, there are two types of normal modes:  $s$ -polarized (TE) and  $p$ -polarized (TM), both of which satisfy the electromagnetic boundary conditions at the guide walls. The total quantized electric and magnetic field operators are written as follows:

$$\begin{aligned} \mathbf{E}(\mathbf{R}_\perp, z, t) = & \sum_{\eta=(p,s)} \sum_{\ell, m} \\ & \times \int_{-\infty}^{\infty} dk \{ a_\eta(k, \ell, m) \mathbf{f}_\eta(k, \ell, m, \mathbf{R}_\perp, z, t) \\ & + \text{H.c.} \}, \end{aligned} \quad (2)$$

$$\begin{aligned} \mathbf{B}(\mathbf{R}_\perp, z, t) = & \sum_{\eta=(p,s)} \sum_{\ell, m} \int_{-\infty}^{\infty} dk \left\{ \left( \frac{1}{i\omega(k, \ell, m)} \right) a_\eta(k, \ell, m) \right. \\ & \left. \times \nabla \mathbf{f}_\eta(k, \ell, m, \mathbf{R}_\perp, z, t) + \text{H.c.} \right\}, \end{aligned} \quad (3)$$

where H.c. stands for ‘‘Hermitean conjugate’’ and we have expressed the position vector in components form by writing  $\mathbf{R} = (\mathbf{R}_\perp, z)$  with  $z$  an axial coordinate and  $\mathbf{R}_\perp = (r, \phi)$  a two-dimensional (transverse) position vector. The operator  $a_\eta(k, \ell, m)$  is the boson operator for the field mode of polarization  $\eta (= p, s)$  characterized by integer quantum numbers  $\ell, m$  and a continuous axial wave vector  $k$ . The relevant commutation relations are

$$[a_\eta(k, \ell, m), a_{\eta'}^\dagger(k', \ell', m')] = \delta_{\eta\eta'} \delta_{\ell\ell'} \delta_{mm'} \delta(k - k'). \quad (4)$$

Finally,  $\mathbf{f}_\eta(k, \ell, m, \mathbf{R}_\perp, z, t)$  are the mode functions for which explicit forms are given below. These vector functions satisfy the wave equation as well as the electromagnetic boundary conditions at the guide walls.

It is convenient to simplify the notation by introducing a compound mode variable  $Q$  which stands for the three mode variables  $(k, \ell, m)$ . The quantized electric field in Eq. (2) becomes

$$\mathbf{E}(\mathbf{R}_\perp, z, t) = \sum_{\eta=(p,s)} \sum_Q \{ a_\eta(Q) \mathbf{f}_\eta(Q, \mathbf{R}_\perp, z, t) + \text{H.c.} \} \quad (5)$$

with a similar equation corresponding to Eq. (3). The sum over  $Q$  stands for one integration over  $k$ , plus two integer sums over  $\ell$  and  $m$ . The mode commutation relations are now given by

$$[a_\eta(Q), a_{\eta'}^\dagger(Q')] = \delta_{\eta\eta'} \delta_{QQ'}, \quad (6)$$

where  $\delta_{QQ'}$  is interpreted by inspection of the right-hand side of Eq. (4).

The mode functions for the transverse magnetic (TM) modes corresponding to  $\eta = p$  ( $p$ -polarized modes) emerge in the form [12]

$$\begin{aligned} \mathbf{f}_p(Q, \mathbf{R}_\perp, z, t) = & C_p(Q) \left( \frac{ik\ell}{h'_{\ell m} r} J_\ell(h'_{\ell m} r) \hat{\phi} - \frac{ik}{h'_{\ell m}} J'_\ell(h'_{\ell m} r) \hat{\mathbf{r}} \right. \\ & \left. + i J'_\ell(h'_{\ell m} r) \hat{\mathbf{z}} \right) e^{\pm i\ell\phi} e^{-i(\omega_p(Q)t - kz)}, \end{aligned} \quad (7)$$

where  $Q$  refers to the three mode variables  $(k, \ell, m)$ ,  $h'_{\ell m} a = \alpha_{\ell m}$  and  $\alpha_{\ell m}$  are the roots of  $J'_\ell(\alpha_{\ell m}) = 0$ . Therefore the dispersion relation  $\omega_p(Q)$  of the TM mode frequency is

$$\omega_p^2(Q) = c^2 \left\{ k^2 + \left( \frac{\alpha_{\ell m}}{a} \right)^2 \right\}. \quad (8)$$

Finally in Eq. (7),  $C_p$  is the  $p$ -polarized mode normalization factor given by

$$C_p(Q) = \left( \frac{c^2 \hbar \alpha_{\ell m}^2}{2N_\ell \varepsilon_0 A L a^2 \omega J_{\ell+1}^2(\alpha_{\ell m})} \right)^{1/2}. \quad (9)$$

Here  $A$  is the cross-sectional area of the guide,  $L$  is its (large) length,  $N_0 = 1$  and  $N_\ell = 1/2$  for  $\ell \neq 0$ .

The second set of electromagnetic modes in the circular waveguide is the transverse electric (TE) set of modes corresponding to  $\eta = s$  ( $s$ -polarized modes). The mode functions for these are [12]

$$\begin{aligned} \mathbf{f}_s(Q, \mathbf{R}_\perp, z, t) = & C_s(Q) \left[ i J'_\ell(h'_{\ell m} r) \hat{\phi} \right. \\ & \left. - \frac{\ell}{h'_{\ell m} r} J_\ell(h'_{\ell m} r) \hat{\mathbf{r}} \right] e^{\pm i\ell\phi} e^{-i(\omega_s(Q)t - kz)}, \end{aligned} \quad (10)$$

where  $h'_{\ell m} a = \beta_{\ell m}$  and  $\beta_{\ell m}$  are the roots of  $J'_\ell(\beta_{\ell m}) = 0$ . Therefore the dispersion relation  $\omega_s(Q)$  of the TE mode frequency is

$$\omega_s^2(Q) = c^2 \left\{ k^2 + \left( \frac{\beta_{\ell m}}{a} \right)^2 \right\}. \quad (11)$$

In Eq. (10)  $C_s(Q)$  is the  $s$ -polarized mode normalization factor, given by

$$C_s(Q) = \left( \frac{\hbar \omega \beta_{\ell m}^2}{2N_\ell \varepsilon_0 A L (\beta_{\ell m}^2 - \ell^2) J_\ell^2(\beta_{\ell m})} \right)^{1/2}. \quad (12)$$

The total Hamiltonian for the electromagnetic fields within the circular waveguide is

$$H_{\text{field}} = \frac{1}{2} \int_{-\infty}^{\infty} dz \int_0^a r dr \int_0^{2\pi} d\phi \left\{ \varepsilon_0 E^2(z, \mathbf{R}_{\perp}, t) + \frac{1}{\mu_0} B^2(z, \mathbf{R}_{\perp}, t) \right\}. \quad (13)$$

The equation  $J_{\ell}(h_{\ell m} a) = 0$  is the dispersion relation for the  $p$ -polarized modes. The following identity involving a definite integral is needed in the analysis:

$$\int_0^a \left\{ J_{\ell}^{\prime 2}(h_{\ell m} r) + \frac{\ell J_{\ell}^2(h_{\ell m} r)}{r^2} \right\} r dr = \frac{a^2}{2} J_{\ell+1}^2(h_{\ell m} r). \quad (14)$$

Also  $J'_{\ell}(h'_{\ell m} a) = 0$  is the dispersion relation of the  $s$ -polarized modes. The following identity also facilitates the analysis:

$$\int_0^a \left\{ J_{\ell}^{\prime 2}(h'_{\ell m} r) + \frac{\ell J_{\ell}^2(h'_{\ell m} r)}{r^2} \right\} r dr = \frac{a^2}{2} \left[ 1 - \left( \frac{\ell}{a} \right)^2 \right] J_{\ell}^2(h'_{\ell m} r), \quad (15)$$

With the help of Eqs. (14) and (15) the factors  $C_p(Q)$  and  $C_s(Q)$  defined in Eqs. (9) and (12) emerge from the usual quantization requirement that the total Hamiltonian  $H_f$  reduces to the canonical form

$$H_{\text{field}} = \frac{1}{2} \sum_{\eta=(p,s)} \sum_Q \hbar \omega(Q) \{ a_{\eta}(Q) a_{\eta}^{\dagger}(Q) + a_{\eta}^{\dagger}(Q) a_{\eta}(Q) \}. \quad (16)$$

### B. Spontaneous emission

The spontaneous decay rate for an electric dipole  $\mathbf{d}$  situated at an arbitrary point  $\mathbf{R} = (\mathbf{R}_{\perp}, z)$  within the waveguide is evaluated using Fermi's golden rule. By symmetry, this rate cannot depend on the axial coordinate  $z$  and we may evaluate it for a dipole situated at an arbitrary point  $(\mathbf{R}_{\perp}, 0)$ , i.e., at a point  $\mathbf{R}_{\perp}$  within the normal cross section of the transverse plane. We have

$$\Gamma(\mathbf{R}_{\perp}) = \frac{2\pi}{\hbar} \sum_{\eta=(p,s)} \sum_Q |\langle e; \{0\} | -\mathbf{d} \cdot \mathbf{E}(\mathbf{R}_{\perp}, 0) | g; \{Q, \eta\} \rangle|^2 \times \delta[E_e - E_g - \hbar \omega_{\eta}(Q)]. \quad (17)$$

The transition from the excited internal state  $|e\rangle$  to the ground state  $|g\rangle$  is effected by the emission of all possible single quanta of waveguide modes with state  $|\{Q, \eta\}\rangle$  of frequency  $\omega_{\eta}(Q)$  and polarization  $\eta$ . The vacuum state is represented by  $|\{0\}\rangle$ .

It should be emphasized that the waveguide frequency spectrum, determined by Eq. (8) for  $p$ -polarized modes and Eq. (11) for  $s$ -polarized modes, comprises two sets of discrete branches, one for each type of polarization  $\eta = (p, s)$ . A frequency branch is labeled by two fixed integers  $\ell$  and  $m$  and within any given branch, the frequency varies only with

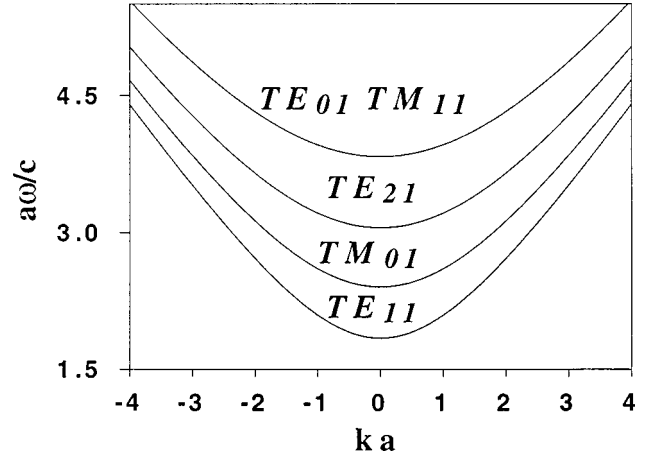


FIG. 2. Dispersion curves showing the TM and TE branches of the guided modes in a cylinder with circular cross section of radius  $a = 0.9\lambda$  where  $\lambda = 589$  nm.

the one-dimensional axial wave vector  $k$ . The TE and TM frequency branches for a typical circular waveguide are shown in Fig. 2.

Depending on the value of the dipole frequency  $\omega_0$ , contributions to the emission rate arise from all branches satisfying the condition

$$\omega_{\eta}(Q) = \omega_{\eta}(k, \ell, m) = \omega_0. \quad (18)$$

Since  $\omega_{\eta}(k, \ell, m)$  depends on the guide radius  $a$  entering via  $h_{\ell m}$  or  $h'_{\ell m}$ , Eq. (18) conceals the dependence on the chosen values of  $a$ .

Assuming a value for  $a$ , the ‘‘zone center’’ ( $k=0$ ) frequency separation between the lowest branch  $\text{TE}_{11}$  corresponding to  $\ell=1, m=1$  and the adjacent branch  $\ell=0, m=1$ , and between the branch  $\text{TM}_{01}$  corresponding to  $\ell=0, m=1$  and the adjacent branch  $\ell=1, m=1$  are approximately given by

$$\Delta \omega_s(01-11) = \omega_s(0,0,1) - \omega_s(0,1,1) = \frac{c}{a} (\beta_{01} - \beta_{11}), \quad (19)$$

$$\Delta \omega_p(11-01) = \omega_p(0,1,1) - \omega_p(0,0,1) = \frac{c}{a} (\alpha_{11} - \omega_{01}). \quad (20)$$

For  $a = 1.0 \mu\text{m}$  we have  $\Delta \omega_s(01-11) \approx 5.97 \times 10^{14} \text{ s}^{-1}$  and  $\Delta \omega_p(11-01) \approx 4.28 \times 10^{14} \text{ s}^{-1}$ . Frequency separations of similar orders of magnitude are obtainable for higher adjacent branches. These frequency separations are therefore quite large for waveguides with dimensions in the micron range. From the special case illustrated in Fig. 2 ( $a = 0.9\lambda$ ,  $\lambda = 589$  nm) we see that if the dipole frequency is equal to  $\omega_s(0,1,1)$ , emission is possible only via the  $\text{TE}_{11}$  ( $\beta_{11} = 1.841$ ) branch. Inspection of Eq. (10) further shows that a dipole oscillating at such a frequency and which is oriented along the axis of the waveguide cannot couple to the electric field of the  $\text{TE}_{11}$  mode and will therefore not decay spontaneously. But spontaneous decay is possible for a dipole ori-

ented along the axis of the waveguide via the  $\text{TM}_{01}$  ( $\alpha_{01} = 2.405$ ) at a frequency less than  $\omega_s(0,0,1)$  and will involve the  $\text{TE}_{11}$  lowest branches as well as the  $\text{TM}_{01}$  branch. If, in addition, this dipole is oriented along the axis, only the  $\text{TM}_{01}$  branch provides a decay channel, since the axial dipole cannot couple to the TE modes. On the other hand, since the branch  $\text{TM}_{11}$  ( $\alpha_{11} = 3.832$ ) coincides with the  $\text{TE}_{01}$  ( $\beta_{01} = 3.832$ ) branch and the  $\text{TE}_{21}$  ( $\beta_{21} = 3.054$ ) branch is below both, the spontaneous decay of a dipole of frequency greater than  $\omega_p(0,1,1)$  will involve the  $\text{TE}_{11}$ ,  $\text{TM}_{01}$ ,  $\text{TE}_{21}$ ,  $\text{TE}_{01}$ , and  $\text{TM}_{11}$  branches. These observations, which are significant for submicron waveguides, are substantiated further with the calculation of the spontaneous rate, as we now show.

The procedure for the calculation of the emission rate based on Eq. (17) can be outlined as follows. Contributions from the  $p$  and  $s$  modes are carried out separately. After evaluating the squared matrix element, use of the dispersion relations, Eq. (8) for  $p$ -polarized modes and Eq. (11) for  $s$ -polarized modes, facilitates the evaluation of the integral over  $k$  involving the  $\delta$  function. We are then left with two sums over integers  $\ell$  and  $m$  and a cutoff condition, Eq. (18), to be satisfied for each evaluation.

### C. Contribution of TM modes

Consider first the evaluation of the contribution from the TM modes which involves use of the mode function defined in Eq. (7). Following the above procedure for the emission rate evaluation in this case culminates in an expression involving sums over  $\ell$  and  $m$ . We have at point  $\mathbf{R}_\perp = (r, \phi)$

$$\Gamma_p(\mathbf{R}_\perp) = \sum_m \left( \frac{d^2}{\pi \hbar \epsilon_0 a^3} \right) \left\{ \frac{\langle d_z \rangle^2}{d^2} G_{\ell m}^z(\mathbf{R}_\perp) + \frac{\langle d_r \rangle^2}{d^2} G_{\ell m}^r(\mathbf{R}_\perp) + \frac{\langle d_\phi \rangle^2}{d^2} G_{\ell m}^\phi(\mathbf{R}_\perp) \right\}, \quad (21)$$

where  $d$  is the magnitude of the dipole matrix element vector  $\langle \mathbf{d}_{12} \rangle$ , with cylindrical components represented by  $\langle d_z \rangle$ ,  $\langle d_r \rangle$ , and  $\langle d_\phi \rangle$ . The  $G$  functions appearing in Eq. (21) are given by

$$G_{\ell m}^z(\mathbf{R}_\perp) = \frac{\alpha_{\ell m}^2}{R_{\ell m} H_{\ell m}} J_\ell^2(h_{\ell m} r), \quad (22)$$

$$G_{\ell m}^r(\mathbf{R}_\perp) = \frac{R_{\ell m}}{H_{\ell m}} J_1^2(h_{\ell m} r), \quad (23)$$

$$G_{\ell m}^\phi(\mathbf{R}_\perp) = \frac{a^2 \ell^2 R_{\ell m}}{\alpha_{\ell m}^2 H_{\ell m}} J_\ell^2(h_{\ell m} r) / r^2, \quad (24)$$

where we have defined  $R_{\ell m}$  and  $H_{\ell m}$  by

$$R_{\ell m} = \left[ \left( \frac{\omega_0 a}{c} \right)^2 - \alpha_{\ell m}^2 \right]^{1/2} \quad \text{and} \quad H_{\ell m} = N_\ell J_{\ell+1}^2(\alpha_{\ell m}). \quad (25)$$

### D. Contribution of TE modes

Similar evaluations leading to the contribution from the  $s$ -polarized modes are based on Eq. (10). The result can be written in the form

$$\Gamma_s(\mathbf{R}_\perp) = \sum_m \left( \frac{d^2 \omega_0^2}{\pi \hbar \epsilon_0 c^2 a} \right) \left\{ \frac{\langle d_r \rangle^2}{d^2} S_{\ell m}^r(\mathbf{R}_\perp) + \frac{\langle d_\phi \rangle^2}{d^2} S_{\ell m}^\phi(\mathbf{R}_\perp) \right\}, \quad (26)$$

where  $S_{\ell m}^r$  and  $S_{\ell m}^\phi$  are given by

$$S_{\ell m}^r(\mathbf{R}_\perp) = \frac{a^2 \ell^2}{R_{\ell m} H_{\ell m}} J_\ell^2(h_{\ell m} r) / r^2, \quad (27)$$

$$S_{\ell m}^\phi(\mathbf{R}_\perp) = \frac{\beta_{\ell m}^2}{R_{\ell m} H_{\ell m}} J_\ell^2(h_{\ell m} r), \quad (28)$$

and we have defined  $R_{\ell m}$  and  $H_{\ell m}$  by

$$R_{\ell m} = \left[ \left( \frac{\omega_0 a}{c} \right)^2 - \beta_{\ell m}^2 \right]^{1/2}$$

and

$$H_{\ell m} = N_\ell (\beta_{\ell m}^2 - \ell^2) J_\ell^2(\beta_{\ell m}), \quad (29)$$

### E. Total spontaneous rate

For a given dipole orientation, the spontaneous emission rate is given by the sum of contributions from the TM and TE sets of modes. The results can be written in terms of  $\lambda$ , the free space transition wavelength. For a dipole oriented along the axis we have

$$\Gamma_z(R_\perp) = \Gamma_0 \sum_m^{[2\pi\sigma]} \frac{3}{(2\pi\sigma)^3} G_{\ell m}^z(\mathbf{R}_\perp). \quad (30)$$

For a dipole oriented along  $\hat{\mathbf{r}}$  we have

$$\Gamma_r(\mathbf{R}_\perp) = \Gamma_0 \frac{3}{(2\pi\sigma)} \left\{ \sum_m^{[2\pi\sigma]} S_{\ell m}^r(\mathbf{R}_\perp) + \sum_m^{[2\pi\sigma]} \frac{1}{(2\pi\sigma)^2} G_{\ell m}^r(\mathbf{R}_\perp) \right\} \quad (31)$$

and for a dipole oriented along  $\hat{\phi}$  we have

$$\Gamma_\phi(\mathbf{R}_\perp) = \Gamma_0 \frac{3}{2\pi\sigma} \left\{ \sum_m^{[2\pi\sigma]} S_{\ell m}^\phi(\mathbf{R}_\perp) + \sum_m^{[2\pi\sigma]} \frac{1}{(2\pi\sigma)^2} G_{\ell m}^\phi(\mathbf{R}_\perp) \right\}, \quad (32)$$

where  $\sigma = a/\lambda$  and  $\Gamma_0$  is the corresponding spontaneous rate in free space

$$\Gamma_0 = \frac{d^2 \omega_0^3}{3 \pi \hbar \epsilon_0 c^3}. \quad (33)$$

These results can now be explored for typical situations involving sodium atoms in circular waveguides. Our main concern here, however, is with the submicron regime ( $a < \lambda$ ). Before we consider this regime, it is instructive to check the results using a particularly simple asymptotic limit arising when the radius  $a$  increases to infinity. As we show next, it is possible to verify by explicit calculations that in this limit the results in Eqs. (30), (31), and (32) yield the spontaneous rate in free space.

### III. SODIUM ATOMS IN SUBMICRON CIRCULAR GUIDES

For orientation as to orders of magnitude, it is instructive to concentrate now on a typical physical situation. We consider the case of a sodium atom and focus on its  $3^2s_{1/2} \leftrightarrow 3^2p_{3/2}$  transition ( $\lambda = 589$  nm). The magnitude of the dipole matrix element associated with this transition is  $d \approx 2.6ea_B$ , which is consistent with the measured free space lifetime of  $\tau \approx 16.3$  ns (or  $\Gamma_0 = 6.13 \times 10^7$  s $^{-1}$ ).

Figure 3 shows the variation of the spontaneous emission rate with the radius of the cylinder for a sodium atom at the center of the cylinder, i.e., at the point  $r=0$ , with the atomic dipole oriented, in turn, along the three directions ( $\hat{\zeta} = \hat{z}, \hat{r}, \hat{\phi}$ ). The plots show the ratio  $\Gamma_{\hat{\zeta}}/\Gamma_0$  against  $a/\lambda$ . For the axial dipole orientation case shown in Fig. 3(a) there is a ‘‘cutoff’’ value of  $a$  below which there is no spontaneous emission. By simple analysis, it is easy to show that the results from Eqs. (31) and (32) are the same at  $r=0$ . In each case the rate oscillates with increasing  $a$ . It is seen that at small values of  $a$  the rate is much higher relative to the free space value for the chosen  $a$  and shows a clear tendency to attaining a fixed value (i.e., the free space value) at large  $a$ .

Figure 4 shows the distribution plots for the spontaneous emission rate when the dipole matrix element has various orientations. The evaluations are carried out for points spanning the guide cross section and are based on the expressions given in Eqs. (30), (31), and (32). Contributions from individual types of mode are not shown. In Figs. 4(a) and 4(c) when the dipole is oriented along  $\hat{z}$  and  $\hat{\phi}$ , respectively, we find that the spontaneous emission rate is zero when the dipole is close to the surface, but when the dipole is oriented along  $\hat{r}$  it is twice the free space value, as shown in Fig. 4(b). These are exactly the values of the spontaneous dipole emission rates at the surface of a single half-space conductor [13]. Indeed, this acts as a useful test for the these results.

As a general rule, however, the spontaneous emission rate is maximum where field components parallel to the dipole matrix element have maximum values. It is also important to note that, because of the subwavelength dimensions ( $a = 0.9\lambda$ ) chosen for illustration purposes in Fig. 4, the emission rate distributions arise from at most five branches of the mode spectrum for a circular guide. This observation is significant for the atom guiding applications to be considered in the next section. Finally, we note that the decay rate of an

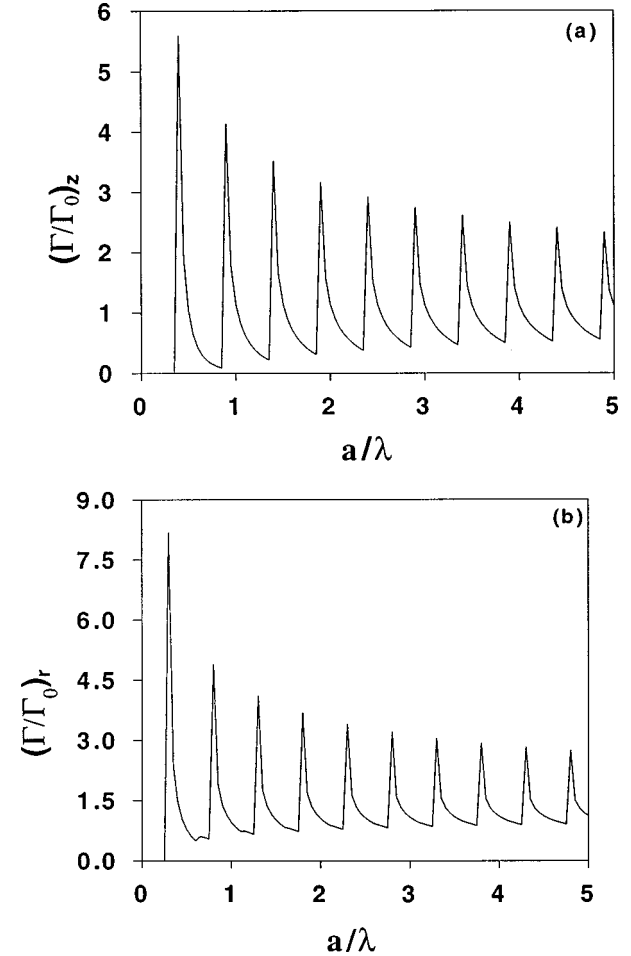


FIG. 3. Total spontaneous emission rate against  $a/\lambda$  (where  $\lambda = 589$  nm) for a sodium atom at the center of the cylinder  $r=0$  when the atomic dipole moment vector is oriented (a) along the  $z$  axis, (b) along the  $\hat{r}$  direction (or  $\hat{\phi}$  direction).

atom in a circular guide depends on three factors: the radius of the guide, the position of the atom, and the orientation of the dipole.

### IV. DYNAMICS

The motion of an atom inside the guide can be altered significantly when a guide mode is excited at frequency  $\omega_{\eta}(Q)$  [where  $Q \equiv (k, \ell, m)$  and  $\eta$  is the polarization type] which is closely tuned to the dipole transition frequency  $\omega_0$ . The total steady state force acting on the center of mass of an atom moving within the guide at velocity  $\mathbf{V}$  due to the excited mode of frequency  $\omega_{\eta}(Q)$  can be written as [1,2]

$$\langle \mathbf{F}_{\eta}(Q, \mathbf{R}, \mathbf{V}) \rangle = 2\hbar \left\{ \frac{\Gamma(\mathbf{R})\Omega^2(\mathbf{R})\nabla\theta(\mathbf{R}) - \frac{1}{2}\Delta(\mathbf{R}, \mathbf{V})\nabla\Omega^2(\mathbf{R})}{\Delta^2(\mathbf{R}, \mathbf{V}) + 2\Omega^2(\mathbf{R}) + \Gamma^2(\mathbf{R})} \right\}_{\eta}, \quad (34)$$

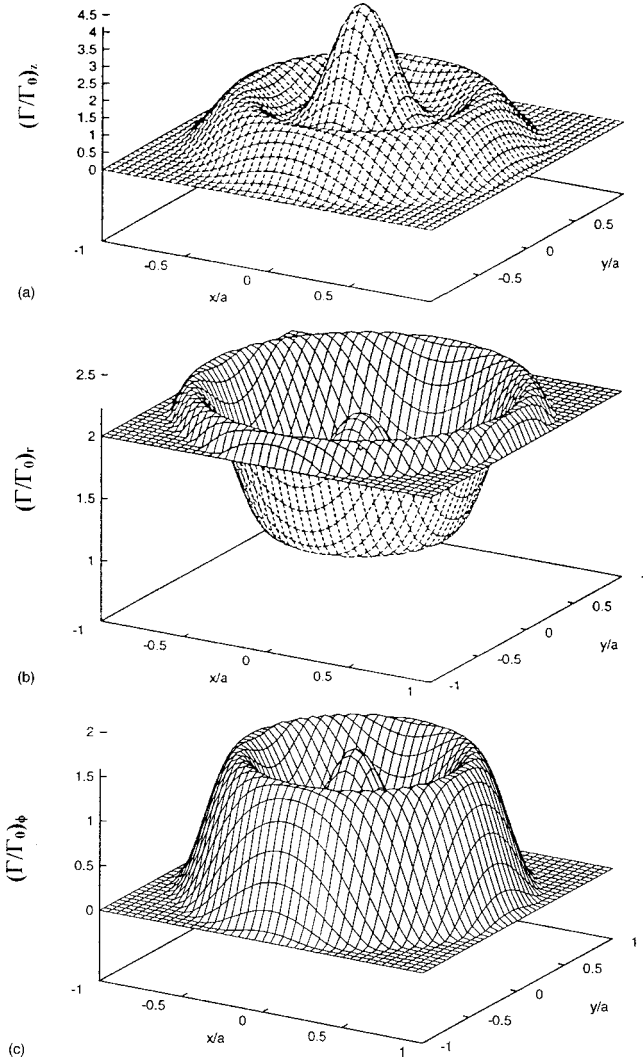


FIG. 4. Distribution plots for the spontaneous emission rate when the dipole matrix element has different orientations for a sodium atom in a cylinder of circular cross section. The plots show the variation of the  $\Gamma/\Gamma_0$  as a function of the position of the atom within the guide: (a) dipole moment vector along the  $z$  direction, (b) along the  $\hat{\mathbf{r}}$  direction, and (c) along the  $\hat{\boldsymbol{\phi}}$  direction.

where  $\Omega$  is the Rabi frequency for an electric dipole  $\mathbf{d}$  in the guide mode whose electric field is defined in Eq. (7) for  $p$ -polarized light, and Eq. (10) for  $s$ -polarized light. It is easy to see that  $\Omega$  is in fact only a function of the radial coordinate  $r$

$$\Omega(\mathbf{R}) = \Omega(r) = \frac{1}{\hbar} |\langle \mathbf{d} \rangle_{eg} \cdot \mathbf{E}|. \quad (35)$$

$\theta_{k\ell}(\mathbf{R})$  is the mode phase which corresponds to the momentum imparted by the light to the atom and, in view of Eqs. (7) and (10), depends only on the axial coordinate  $z$  and the azimuthal coordinate  $\phi$  and is written as

$$\theta_{k\ell} = \ell\phi + kz. \quad (36)$$

Thus  $\theta_{k\ell}$  has the gradient

$$\nabla \theta_{k\ell} = \frac{\ell}{r} \hat{\boldsymbol{\phi}} + k\hat{\mathbf{z}}. \quad (37)$$

This immediately shows that the dissipative force has components in both the axial and azimuthal directions.  $\Delta(\mathbf{R}, \mathbf{V})$  is a dynamic detuning which is a function of both the position and the velocity vectors of the atom

$$\Delta_\eta(Q, \mathbf{R}, \mathbf{V}) = \Delta_0 - \mathbf{V} \cdot \nabla \theta_{k\ell} \quad (38)$$

with  $\Delta_0 = \omega_\eta(Q) - \omega_0$  the static detuning of the guide mode from the atomic resonance.

### A. Doppler shift

The second term in Eq. (38)  $\delta = -\mathbf{V} \cdot \nabla \theta_{k\ell}$  represents the Doppler shift due to the excited mode. On making use of Eq. (37), we have

$$\delta(\mathbf{r}, \mathbf{V}) = -kV_z - \frac{\ell V_\phi}{r}, \quad (39)$$

where  $V_z$  and  $V_\phi$  are the axial and azimuthal components of the atomic velocity vector. The first term in  $\delta$  is the expected Doppler shift that would arise for a plane wave traveling along the axis of the cylinder. The second term can be written as

$$\delta_\phi(r, V_\phi) = -\ell\omega_r, \quad (40)$$

where  $\omega_r = V_\phi/r$  is the angular velocity of the atom. This has the same form as the rotational shift discussed in a recent article by Bialynicki-Birula and Bialynicka-Birula [14] who predicted that a rotating quantum system undergoing spontaneous emission is subject to a frequency shift equal to  $l\omega_r$  where  $\omega_r$  is its angular frequency and  $l$  is the angular momentum of the emitted light. The rotational shift of Ref. [14] had also been the subject of investigation by Silverman [15] and has been used in the discussion of the mechanical Faraday effect [16]. The shift has the same form discussed more recently by Courtial *et al.* [17] who observed a frequency shift  $\ell\omega_r$  for a free space Laguerre-Gaussian light beam of orbital angular momentum quantum number  $\ell$  when the beam is rotated about its axis at an angular frequency  $\omega_r$ . The interesting feature here is that the frequency shift is quantized in units of the quantum number  $\ell$ , but the first effect concerns the orbital motion of the radiating system, while the second the orbital angular momentum of the light.

Here we show that interesting rotational effects can also be induced by light on quantum systems, not in free space, but in the context of atom guides. As has been pointed out, cylindrical structures with circular cross section can act as waveguides to both atoms and light in mutual interaction [18]. The mechanical effects on material objects due to the angular momentum of microwave photons confined in circular waveguides has been pointed out by Kristensen *et al.* [19]. In the context of atoms, it is the orbital angular momentum property associated with the azimuthal dependence of the field structure that is responsible for the new effects emerging in the interaction of the atom with a waveguide

mode of order greater than the fundamental mode. We show here that this gives rise to a number of rotational features which make the atomic motion drastically different from that associated with the fundamental mode of the waveguide.

The interpretation of the shift in Eq. (40) in this case can be easily made in terms of angular momentum  $\ell\hbar$  carried by a quantum (photon) of the waveguide mode. Note, however, that the shift does not depend on the frequency of the mode, only on its order  $\ell$ , which coincides with the orbital angular momentum quantum number of the mode. Equation (40) can be rewritten in Cartesian coordinates in the form

$$\delta_\phi(r, V_\phi) = - \left( \frac{-\ell y}{r^2} V_x + \frac{\ell x}{r^2} V_y \right). \quad (41)$$

Since the total Doppler shift is the dynamic (i.e., velocity-dependent) part of the detuning  $\Delta_\eta(Q)$  which enters the total force in Eq. (34), it clearly has an important role to play in the dynamics of the atom within the cylindrical guide.

### B. Radiation forces and torque

Another context where the phase gradient enters is the first term of the force field given in Eq. (34). Substituting for  $\nabla\theta$  from Eq. (37), the first term of the force field (the dissipative force) can be written as

$$\langle \mathbf{F}_\eta(Q, \mathbf{R}, \mathbf{V}) \rangle_{\text{diss}} = 2\hbar \left\{ \frac{\Gamma(r)\Omega^2(r)[(\ell/r)\hat{\phi} + k\hat{z}]}{\Delta^2(\mathbf{R}, \mathbf{V}) + 2\Omega^2(r) + \Gamma^2(r)} \right\}_\eta. \quad (42)$$

As Eq. (42) suggests, to influence the atom in the azimuthal direction, the integer  $\ell$  must be greater than zero, otherwise the atom will only be subject to a force in the axial direction. The axial component of the dissipative force can be written as

$$\langle F_{\eta(z)}(Q, \mathbf{R}, \mathbf{V}) \rangle_{\text{diss}} = 2\hbar k \left\{ \frac{\Gamma(r)\Omega^2(r)}{\Delta^2(\mathbf{R}, \mathbf{V}) + 2\Omega^2(r) + \Gamma^2(r)} \right\}_\eta \quad (43)$$

and the azimuthal component of the dissipative force involving the orbital angular momentum is given by

$$\langle F_{\eta(\phi)}(Q, \mathbf{R}, \mathbf{V}) \rangle_{\text{diss}} = \frac{2\ell\hbar}{r} \left\{ \frac{\Gamma(r)\Omega^2(r)}{\Delta^2(\mathbf{R}, \mathbf{V}) + 2\Omega^2(r) + \Gamma^2(r)} \right\}_\eta. \quad (44)$$

This force field component is thus responsible for a torque  $\mathbf{T}_\eta$  acting on the atom center of mass about the axis of the cylinder which is given by

$$\mathbf{T}_\eta(Q, \mathbf{R}, \mathbf{V}) = \hat{z} \langle r F_\phi \rangle_\eta = \left\{ \frac{2\ell\hbar\Gamma(r)\Omega^2(r)}{\Delta^2(\mathbf{R}, \mathbf{V}) + 2\Omega^2(r) + \Gamma^2(r)} \right\}_\eta \hat{z}. \quad (45)$$

It is easy to check that this torque depends only on the radial coordinate. In addition, it depends on the atom velocity vector  $\mathbf{V}$ . In the saturation limit, corresponding to large  $\Omega$ , one obtains for the magnitude of this light torque

$$T_\eta \approx \ell\hbar\Gamma_\eta(r). \quad (46)$$

This result has the simple interpretation that for an atom at the radial point  $r$  the mode supplies angular momentum  $\ell\hbar$  delivered at the rate of  $\Gamma_\eta(r)$  quanta per second and thus gives rise to a rate of angular momentum per second equal to the product  $\ell\hbar\Gamma_\eta$ , that is the torque acting on the atom about the cylinder axis. If  $\Gamma$  were not position and mode dependent, the result could have been interpreted as a torque quantized in unit of  $\hbar\Gamma$ . As we now show, the position and mode dependence as well as the velocity dependence, which are manifest in the general result in Eq. (45), make the dynamics of atoms in waveguides significantly different from other situations. The torque effects due to different kinds of light on atoms has been discussed by van Enk and van Enk and Nienhaus [20] and atom dynamics in free space Laguerre-Gaussian beams have also been reported [21–23].

On the other hand, the second term of the force field (the dipole force) given in Eq. (34), can be written as

$$\langle \mathbf{F}_\eta(Q, \mathbf{R}, \mathbf{V}) \rangle_{\text{dipole}} = \left\{ \frac{-\hbar\Delta(\mathbf{R}, \mathbf{V})\nabla\Omega^2(r)}{\Delta^2(\mathbf{R}, \mathbf{V}) + 2\Omega^2(r) + \Gamma^2(r)} \right\}_\eta. \quad (47)$$

This means that the atoms also become subject to a light-induced dipole force and this, too, depends on the dipole orientation as well as the type of cavity mode. The explicit form of the dipole potential for a waveguide mode characterized by  $Q$  and  $\eta$  is such that  $\langle \mathbf{F}_\eta \rangle_{\text{dipole}} = -\nabla U_\eta$ , with  $U_\eta$  in this case written as

$$U_\eta(Q, \mathbf{R}, \mathbf{V}) = \left\{ \left( \frac{\hbar\Delta(\mathbf{R}, \mathbf{V})}{2} \right) \ln \left[ 1 + \frac{2\Omega^2(r)}{[\Delta^2(\mathbf{R}, \mathbf{V}) + \Gamma^2(r)]} \right] \right\}_\eta. \quad (48)$$

It is clear that the potential will exhibit a minimum (maximum) at the high intensity locations where  $\Delta_\eta < 0$  ( $\Delta_\eta > 0$ ).

### C. Equation of motion

The dynamics of an atom of mass  $M$  immersed in the waveguide mode of frequency  $\omega_\eta(Q)$  follows straightforwardly by solving the equation of motion subject to the force in Eq. (34), namely,

$$M \left( \frac{d^2\mathbf{R}}{dt^2} \right)_\eta = \langle \mathbf{F}_\eta(Q, \mathbf{R}, \mathbf{V}) \rangle, \quad (49)$$

We have not included the effects of the van der Waals potential, appropriate for the subwavelength dimensions, since its role for atoms in cavities has been clarified, both experimentally [24] and theoretically [1]. In particular, the van der Waals potential is expected to be effective only at a relatively short distance from the guide surfaces. In general, by using Eqs. (42) and (47), the equation of motion (49) can be rewritten as (dropping the  $\eta$  and  $Q$  mode labels for convenience)

$$\begin{aligned} \left(\frac{d^2\mathbf{R}}{dt^2}\right) &= \left(\frac{d\mathbf{V}}{dt}\right) \\ &= \frac{2\hbar}{M} \left\{ \Gamma\Omega^2 \left( \frac{(k\hat{\mathbf{z}}) + (\ell/r)}{\Delta^2 + 2\Omega^2 + \Gamma^2} \right) \right. \\ &\quad \left. - \Omega \frac{\partial\Omega}{\partial r} \left( \frac{\Delta}{\Delta^2 + 2\Omega^2 + \Gamma^2} \right) \hat{\mathbf{r}} \right\} \end{aligned} \quad (50)$$

which can be expressed as two equations, describing longitudinal and transverse components of the motion as follows:

$$\left(\frac{dV_z}{dt}\right) = \left(\frac{d^2z}{dt^2}\right) = \frac{1}{M} \left\{ \frac{2\hbar k\Gamma\Omega^2}{\Delta^2 + 2\Omega^2 + \Gamma^2} \right\}, \quad (51)$$

$$\begin{aligned} \left(\frac{d\mathbf{V}_\perp}{dt}\right) &= \left(\frac{d^2\mathbf{R}_\perp}{dt^2}\right) \\ &= \frac{2\hbar}{M} \left\{ \Gamma\Omega^2 \left( \frac{(\ell/r)}{\Delta^2 + 2\Omega^2 + \Gamma^2} \right) \hat{\phi} \right. \\ &\quad \left. - \Omega \frac{\partial\Omega}{\partial r} \left( \frac{\Delta}{\Delta^2 + 2\Omega^2 + \Gamma^2} \right) \hat{\mathbf{r}} \right\}. \end{aligned} \quad (52)$$

Equation (52) can be split into two equations as follows:

$$\left(\frac{dV_\phi}{dt}\right) = \frac{2\hbar}{M} \left\{ \Gamma\Omega^2 \left( \frac{(\ell/r)}{\Delta^2 + 2\Omega^2 + \Gamma^2} \right) \right\}, \quad (53)$$

$$\left(\frac{dV_r}{dt}\right) = \frac{2\hbar}{M} \left\{ -\Omega \frac{\partial\Omega}{\partial r} \left( \frac{\Delta}{\Delta^2 + 2\Omega^2 + \Gamma^2} \right) \right\}. \quad (54)$$

Thus we now have three components of motion; the axial motion Eq. (51), the azimuthal motion Eq. (53), and the radial motion Eq. (54). These are coupled motions since  $\Delta$  contains dependence on all three components of  $\mathbf{V}$ . In Eqs. (53) and (54) we can alternatively express the motion in terms of the  $x$  and  $y$  variables as follows:

$$\begin{aligned} \left(\frac{d^2x}{dt^2}\right) &= \left(\frac{dV_x}{dt}\right) = -\frac{2\hbar}{M(\Delta^2 + 2\Omega^2 + \Gamma^2)} \left[ \Gamma\Omega^2 \frac{\ell y}{r^2} \right. \\ &\quad \left. + \Omega \frac{\partial\Omega}{\partial r} \Delta \frac{x}{r} \right], \end{aligned} \quad (55)$$

$$\begin{aligned} \left(\frac{d^2y}{dt^2}\right) &= \left(\frac{dV_y}{dt}\right) = \frac{2\hbar}{M(\Delta^2 + 2\Omega^2 + \Gamma^2)} \left[ \Gamma\Omega^2 \frac{\ell x}{r^2} \right. \\ &\quad \left. - \Omega \frac{\partial\Omega}{\partial r} \Delta \frac{y}{r} \right], \end{aligned} \quad (56)$$

where we have used  $\hat{\phi} = (-\sin\phi)\hat{\mathbf{x}} + (\cos\phi)\hat{\mathbf{y}}$ ,  $\hat{\mathbf{r}} = (\cos\phi)\hat{\mathbf{x}} + (\sin\phi)\hat{\mathbf{y}}$ ,  $\sin\phi = y/r$ ,  $\cos\phi = x/r$ , and  $r = \sqrt{x^2 + y^2}$ .

It is thus clear that Eq. (49) constitutes a set of three coupled ordinary differential equations. These, for a given set of initial conditions, can be solved numerically using standard routines.

## V. ATOM MOTION

### A. Typical parameters

In order to exhibit the salient features of the dynamics, it is necessary to consider a specific physical situation in which sodium atoms are guided along a circular waveguide in which the  $\text{TM}_{11}$  mode has been excited by a laser of intensity  $I \approx 10^7 \text{ W m}^{-2}$  which is the laser intensity adopted by Renn *et al.* in their experiment [9]. We focus again on the transition at  $\lambda = 589 \text{ nm}$  and we define a free space Rabi frequency  $\Omega_0$  by

$$\Omega_0 = \left( \frac{Id^2}{2\hbar^2 \epsilon_0 c} \right)^{1/2} \approx 8.56 \times 10^9 \text{ s}^{-1}. \quad (57)$$

We assume a waveguide of radius  $a = 0.9\lambda$  and a static detuning  $\Delta_0 \approx -35.76 \text{ MHz}$ , which is much smaller than a typical zone-center frequency spacing. We also introduce two scaling parameters: a scaling force  $F_0$  and a scaling potential  $U_0$ . With integers  $\ell$ ,  $m$  known,  $\Delta_0$  as defined above and with  $\omega_0$  corresponding to  $\lambda = 589 \text{ nm}$ , it is straightforward to deduce the magnitude of the axial wave vector  $k$  ( $k$  depends on the kind of excited mode;  $p$  or  $s$  polarized) and on the order of the mode  $\ell m$ . Consequently, Eq. (8) is used when the  $\text{TM}_{11}$  mode ( $\alpha_{11} = 3.832$ ) is excited. The scaling parameter  $F_0$  for this  $k_{11}$  is defined by

$$F_0 = 2\hbar k_{11} \Gamma_0 \approx 1.16 \times 10^{-19} \text{ N}. \quad (58)$$

The scaling potential energy  $U_0$  for all modes is defined by

$$U_0 = (1/2)\hbar\Gamma_0 = 3.13 \times 10^{-27} \text{ J} \approx 4.7 \text{ MHz}. \quad (59)$$

In the figures below, force is measured in units of  $F_0$  and potential energy in units of  $U_0$ .

We focus now on the three possible cases of dipole orientation separately by assuming that the electric dipole is oriented in a fixed direction. First we assume that the electric dipole is *parallel* to the cylinder axis (i.e., along the axial direction). Second, we consider the case when it is *perpendicular* to the cylinder axis (i.e., along the radial direction) and finally when it is oriented in the *azimuthal* direction.

### B. Dipole along axis ( $\hat{\mathbf{z}}$ )

With the dipole oriented along the axis ( $\hat{\mathbf{z}}$  direction) and with the  $\text{TM}_{\ell m}$  mode excited we have a position-dependent Rabi frequency given by

$$[\Omega_p(k, \ell, m, r)]_z = \Omega_0 \frac{\alpha_{\ell m} c \left| J_\ell \left( \alpha_{\ell m} \frac{r}{a} \right) \right|}{a \omega_0 \sqrt{N_\ell} |J_{\ell+1}(\alpha_{\ell m})|}. \quad (60)$$

Figure 5 displays the spatial distribution of this Rabi frequency over a diameter of the cross section of the guide when the  $\text{TM}_{11}$  mode with a Rabi frequency  $[\Omega_p(k, 1, 1, r)]_z$  is excited. The maximum intensity is located at points where  $r = a/2$ . Therefore the potential will exhibit a minimum at these points for  $\Delta_0 < 0$ . For  $\Delta_0 > 0$  we have trapping at the low intensity (dark) regions of the field. With the dipole

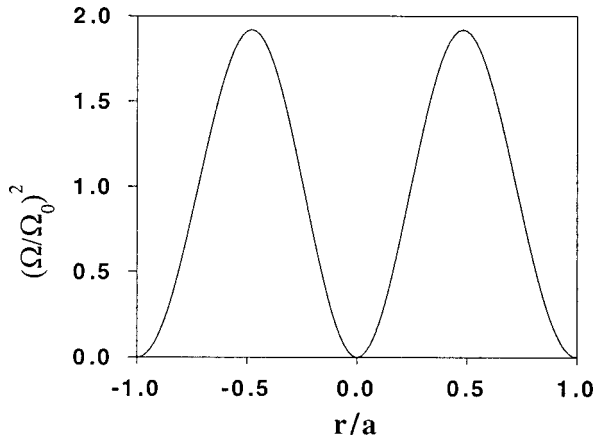


FIG. 5. Variation of the square of the Rabi frequency within a central cross section of the guide for a sodium atom when the  $TM_{11}$  mode is excited. Here the electric dipole moment vector is axial.

oriented along the axis and in a situation corresponding to the above choice of parameters, the axial component of the dissipative force field given by Eq. (43) is set up with spatial distribution over a diameter of the cross section of the guide, as depicted in Fig. 6. It can be seen from this figure that atoms located at  $r = a/2$  experience the strongest force along the axis.

The corresponding profile of the dipole potential  $(U_p(x,y))_z$  is depicted in Fig. 7(a). As expected, we see that for  $\Delta_0 < 0$  the dipole potential exhibits a minimum at points where the intensity is maximum. A reversal of the sign of detuning, obviously, leads to the dipole potential of the opposite sign to that depicted in Fig. 7(a) and it is easy to see that transverse trapping of atoms is also possible for this case, as shown in Fig. 7(b). It can be deduced from these figures that, from a quantum-mechanical point of view, solutions of the two-dimensional Schrödinger equation with  $[U_p(x,y)]_z$  as potential must exist. In the ground state, the atomic wave function peaks in the vicinity of the central minimum associated with the dipole potential. It can also be

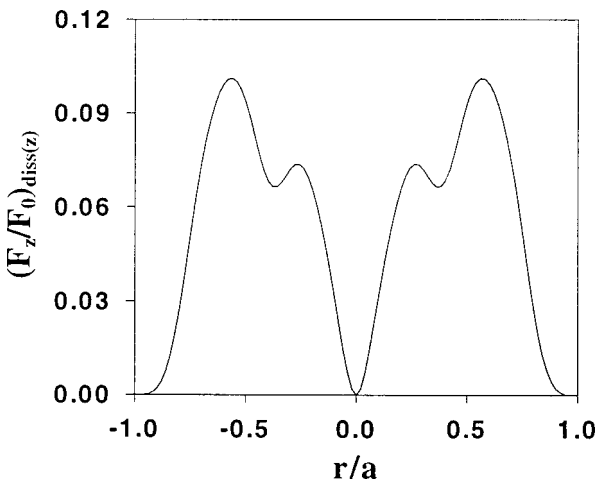


FIG. 6. Variation of the axial quasistatic dissipative force acting on a sodium atom when the  $TM_{11}$  mode is excited. Here the electric dipole moment vector is axial.

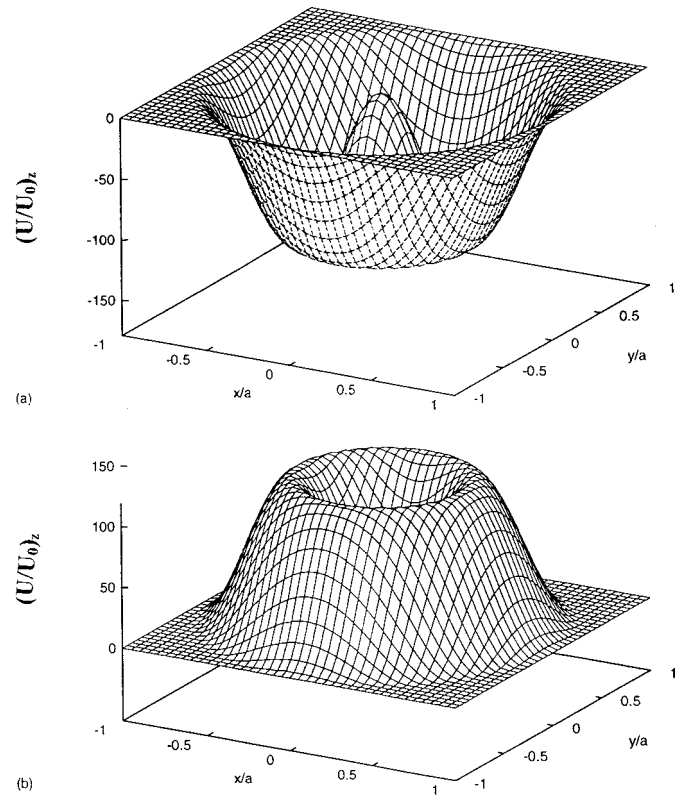


FIG. 7. Spatial distribution of the potential of the sodium atom in the circular waveguide under the conditions of Fig. 6 when the dipole moment vector is along the cylinder axis; (a) negative detuning, (b) positive detuning.

seen from Fig. 7(a) that for the parameters assumed above, the central well depth is approximately  $(118U_0 \approx 0.557 \text{ GHz})$ . This is sufficiently deep to exhibit many quasiharmonic trapping (vibrational) states. The vibrational frequency can be estimated simply using the parabolic approximation [1,2].

Figures 8 shows the projection of the trajectory on the  $xy$  plane based on the solution of Eq. (49) for an atom with its electric dipole moment vector oriented parallel to the cylinder axis in the presence of the  $TM_{11}$  mode of the waveguide, assuming negative detuning with the initial conditions such that the atom starts from rest at the point  $x = y = 0.5a$ . This leads to the interpretation of the motion as the sum of radial and rotational motions superimposed on a translational motion along the axis (not shown). The rotational motion is an expected signature of the light torque effects mentioned above, while the translational motion along the axis (not shown) is due to the pressure force acting along the direction of propagation. The radial features of the trajectory immediately suggest that the atom may be trapped in an annulus-shaped quantum well due to the light and this is confirmed by inspecting the distribution of the dipole potential associated with Eq. (48) for the negative detuning situation, as shown in Fig. 7(a). The evolution of velocity components can also be displayed and it is found that the axial velocity  $V_z$  grows in magnitude with time while the transverse velocities ( $V_x$  and  $V_y$ ) exhibit periodic oscillations.

On the other hand, the radial features of the corresponding trajectory shown in Fig. 9 for the positive detuning case  $\Delta_0$

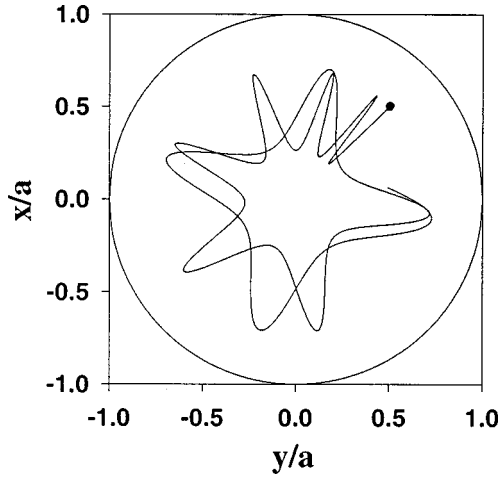


FIG. 8. Predicted trajectory of a sodium atom on a transverse ( $xy$ ) plane of a subwavelength cylindrical guide. The atomic dipole is assumed to remain in the axial direction in the presence of an excited  $TM_{11}$  mode of the guide for the negative detuning case. See text for values of parameters.

$>0$  immediately suggest that the atom must be trapped in a bowl-shaped quantum well due to the light and this is confirmed by inspecting the distribution of the dipole potential associated with Eq. (48) for the positive detuning situation, as in Fig. 7(b).

**C. Dipole along ( $\hat{r}$ )**

With the dipole oriented transversely along the  $\hat{r}$  direction and with the  $TM_{lm}$  mode excited, the corresponding Rabi frequency is obtained as

$$(\Omega_p(k, \ell, m, r))_r = \Omega_0 \frac{kc \left| J'_\ell \left( \alpha_{\ell m} \frac{r}{a} \right) \right|}{\omega_0 \sqrt{N_\ell} |J_{\ell+1}(\alpha_{\ell m})|}. \quad (61)$$

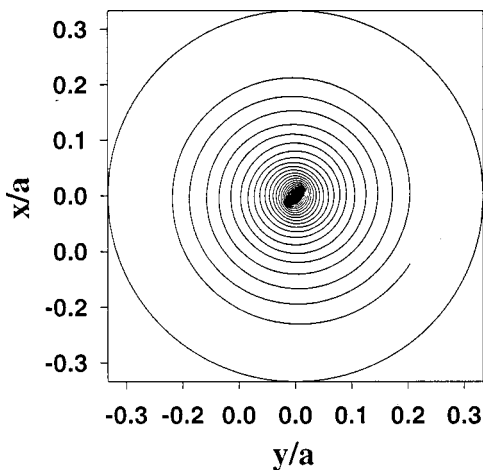


FIG. 9. (a) Predicted projection in the  $xy$  plane of the trajectory of a sodium atom in a subwavelength cylindrical guide. The atomic dipole is assumed to remain in the axial direction in the presence of an excited  $TM_{11}$  mode of the guide for the positive detuning case. The initial conditions are such that the atom starts from rest at  $x=0=y$ . See text for values of parameters.

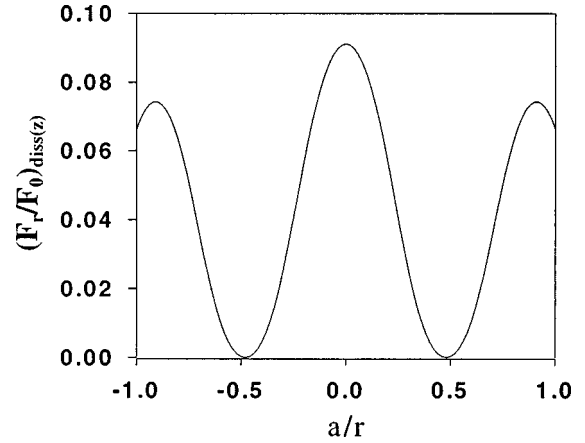


FIG. 10. Variation of the axial quasistatic dissipative force acting on a sodium atom when the  $TM_{11}$  mode is excited. Here the electric dipole moment vector is oriented (transversely) along the  $\hat{r}$  direction.

The quasistatic axial component of the dissipative force field given by Eq. (43), corresponding to the same choice of parameters as in the previous subsection, is shown in Fig. 10 for a dipole oriented along the  $\hat{r}$  direction. It can be seen from this figure that atoms located at the center ( $r=0$ ) of the guide experience the strongest force along the axis and at the wall ( $r=a$ ), while atoms located at  $r=a/2$  of the guide do not experience any force. The corresponding profile of the dipole potential  $[U_p(x, y)]_r$  is depicted in Fig. 11(a). A re-

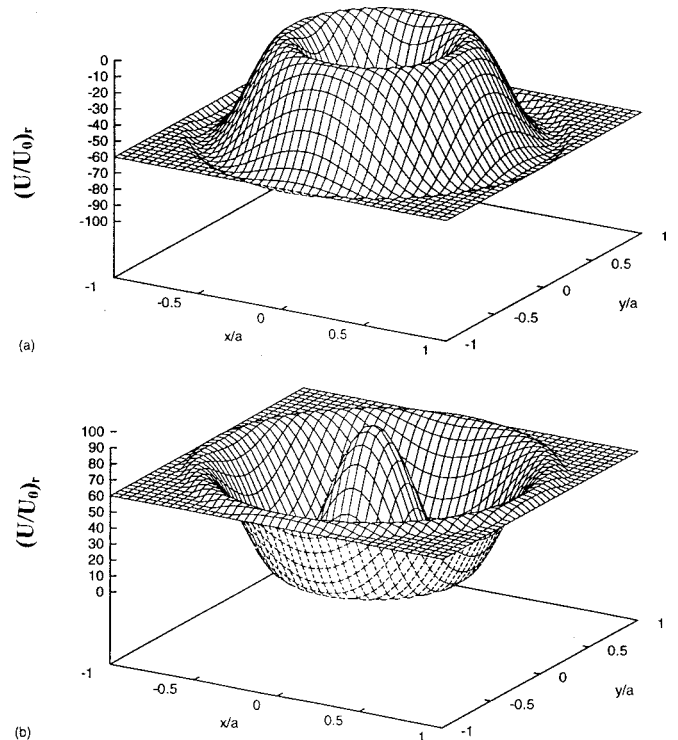


FIG. 11. Spatial distribution of the dipole potential on the sodium atom in the circular waveguide under the conditions of Fig. 10 when the dipole is along the  $\hat{r}$  direction; (a) negative detuning, (b) positive detuning.

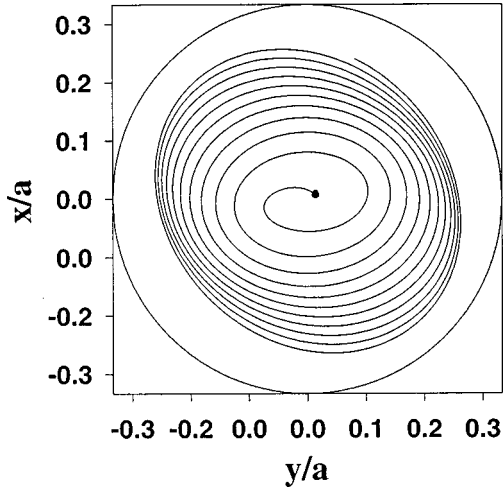


FIG. 12. Predicted trajectory in the  $xy$  plane for a sodium atom in a subwavelength cylindrical guide. The atomic dipole is assumed to remain radial in the presence of an excited  $TM_{11}$  mode of the guide for the negative detuning case. See the text for values of parameters.

versal of the sign of detuning, however, leads to the dipole potential shown in Fig. 11(b) of the opposite sign and it is easy to see that transverse trapping of atoms is also possible for this case. The solutions of the two-dimensional Schrödinger equation with  $[U_p(x,y)]_r$  as potential must also exist and the central well depth is approximately  $(90U_0)$ . This, too, is sufficiently deep to allow several quasiharmonic trapping (vibrational) states.

Figure 12 displays the projection of the trajectory when the electric dipole moment vector is oriented perpendicular to the cylinder axis in the presence of the  $TM_{11}$  mode for the negative detuning situation. The initial conditions are such that the atom starts from rest at  $x=y\approx 0$ . As in the previous section, Fig. 12 leads to the interpretation of the motion as the sum of radial and rotational motions superimposed on a translational motion along the axis. The rotational motion is an expected signature of the light torque effects, while the translational motion along the axis is due to the pressure force acting along the axis. The radial features of the trajectory immediately suggest that the atom must be trapped in a bowl-shaped quantum well due to the light and this is confirmed by inspecting the distribution of the dipole potential associated with Eq. (48) for the negative detuning situation, as shown in Fig. 11(a).

Figure 13 displays the trajectory projection onto the  $x-y$  plane when the electric dipole moment vector is oriented perpendicular to the cylinder axis in the presence of the  $TM_{11}$  mode, for the positive detuning situation. The initial conditions are such that the atom starts from rest at the  $x=y=0.5a$ . The radial features of the trajectory for the atom in the positive detuning case immediately suggest that the atom is trapped in an annulus-shaped quantum well due to the light and this is confirmed by inspecting the distribution of the dipole potential associated with Eq. (48), as shown in Fig. 11(b).

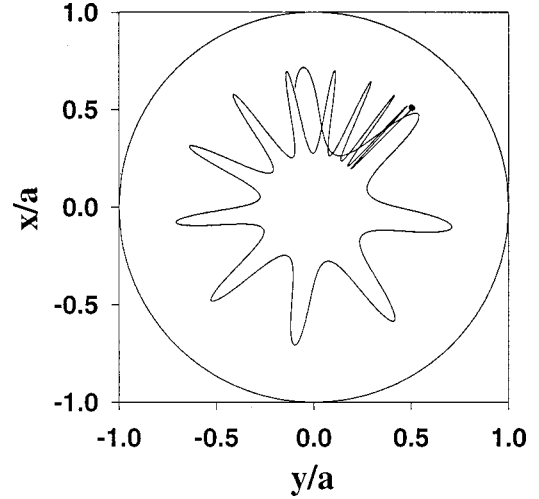


FIG. 13. Predicted trajectory of a sodium atom on the transverse ( $xy$ ) plane of a subwavelength cylindrical guide. The atomic dipole is assumed to remain radial in the presence of an excited  $TM_{11}$  mode of the guide for the positive detuning case. See the text for values of parameters.

#### D. Dipole along $\hat{\phi}$

With the dipole oriented along the  $\hat{\phi}$  direction and with the  $TM_{lm}$  mode excited, the corresponding Rabi frequency is given by

$$[\Omega_p(k,l,m,r)]_\phi = \Omega_0 \frac{k/c a \left| J_l \left( \alpha_{l,m} \frac{r}{a} \right) / r \right|}{\omega_0 \alpha_{l,m} \sqrt{N_l} |J_{l+1}(\alpha_{l,m})|}. \quad (62)$$

The maximum of the Rabi frequency is located at points where  $r=0$  and so the dipole potential will exhibit a minimum at this point for  $\Delta_0 < 0$ . The quasistatic axial component of the dissipative force, given by Eq. (43) (for the same choice of parameters as in the previous subsection) is shown in Fig. 14. The corresponding potential  $(U_p(x,y))_\phi$  is dis-

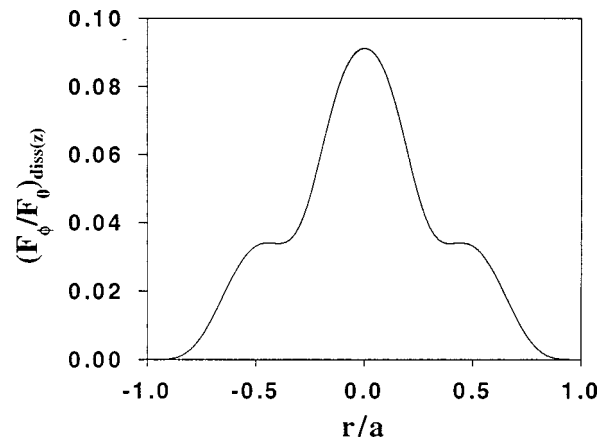


FIG. 14. Variation of the axial quasistatic dissipative force acting on a sodium atom along a diameter when the  $TM_{11}$  mode is excited. Here the electric dipole moment vector is oriented along the  $\hat{\phi}$  direction.

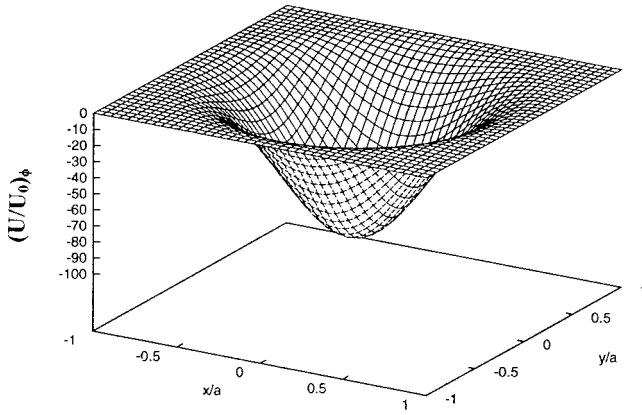


FIG. 15. Spatial distribution of the potential of the sodium atom in the circular waveguide under the conditions of Fig. 14 when the dipole is along the  $\hat{\phi}$  direction and for negative detuning.

played in Fig. 15. Here the dipole potential for this component has a minimum at the center of the guide for negative detuning. The solutions of the two-dimensional Schrödinger equation with  $[U_p(x,y)]_\phi$  as potential must exist too and the central well depth is approximately  $85U_0$ , which is also sufficiently deep to allow several quasiharmonic trapping states. In contrast to the case of negative detuning, the dipole potential for the positive detuning case has no minimum at the center of the guide. In fact, in the positive detuning case the atoms tend to be attracted towards the cylinder wall. In other words, the solution of Schrödinger equation with  $[U_p(x,y)]_\phi$  as potential for positive detuning will always have the atomic vibrational ground state distribution peaking in the vicinity of the wall. From the point of view of atom guiding, such a dipole orientation will not result in efficient atom guiding by the  $TM_{11}$  mode with positive detuning.

Figure 16 shows the trajectory for an atom with its electric dipole moment vector oriented along the  $\hat{\phi}$  direction in the presence of the  $TM_{11}$  mode of the waveguide in the

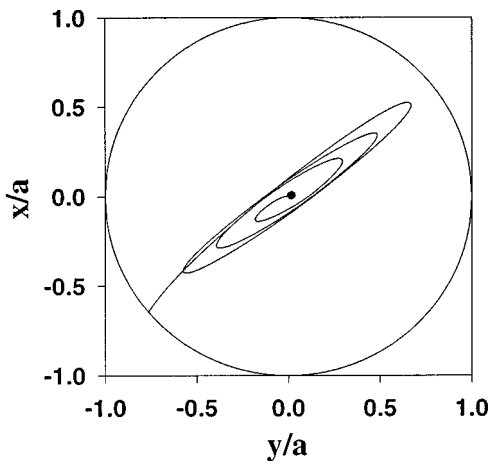


FIG. 16. Predicted trajectory of a sodium atom on a transverse  $(xy)$  plane of a subwavelength cylindrical guide. The atomic dipole is assumed to remain in the  $\hat{\phi}$  direction in the presence of an excited  $TM_{11}$  mode in the guide for the negative detuning case. See the text for values of parameters.

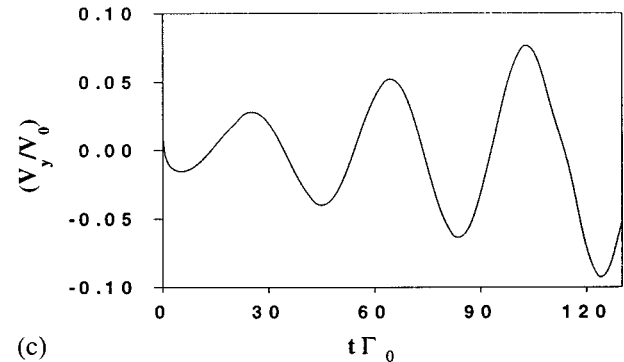
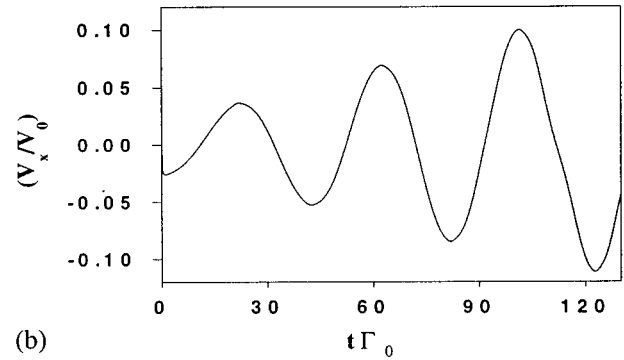
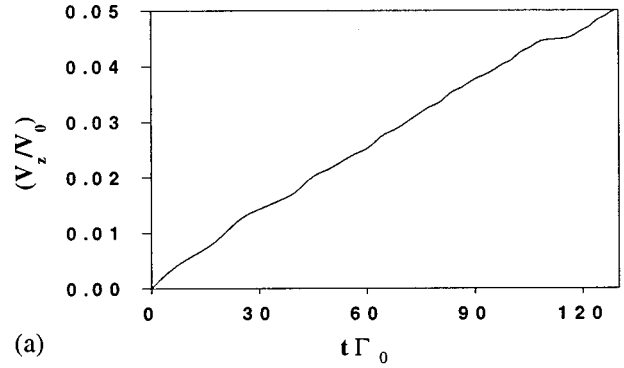


FIG. 17. Variations of the velocity components for the case in Fig. 16: (a) evolution of  $V_z$ ; (b) evolution of  $V_x$ ; (c) evolution of  $V_y$ . Both (b) and (c) indicate the onset of oscillatory motions of the same time scale. All velocities are in unit of  $V_0 = a\Gamma_0$ .

negative detuning case, with the initial conditions such that the atom starts from rest at  $x=y \approx 0$ . This figure leads to the interpretation of the motion as the sum of radial and rotational motions superimposed on a translational motion along the axis. The radial features of the trajectory immediately suggest that the atom is trapped in a bowl-shaped quantum well due to the light and this is confirmed by inspecting the distribution of the dipole potential associated with Eq. (48), as shown in Fig. 15. The potential distribution, in fact, changes with the axial velocity in that the depth of the well decreases with increasing axial velocity. Figure 17 displays the evolution of the velocity components. The axial velocity ( $V_z$ ) is seen to grow with time, as depicted in Fig. 17(a),

while the transverse velocities ( $V_x$  and  $V_y$ ) exhibit periodic oscillations as can be seen in Figs. 17(b) and 17(c), respectively.

## VI. COMMENTS AND CONCLUSIONS

In conclusion, we have examined in detail the cavity QED of atoms in cylindrical waveguides with circular cross sections. The cavity modes are first quantized by following the standard procedure, incorporating the boundary conditions at the guide walls. This allowed the position-dependent spontaneous emission rate to be evaluated for an electric dipole within the guide. In addition to its intrinsic value, the spontaneous emission rate in these structures is important for the theory of atom guides. Useful limits of the spontaneous emission rate have been derived. In particular, we have been able to recover the results appropriate for the free space case when the radius  $a$  of the guide becomes large.

We have explored the details of atom dynamics inside cylindrical perfect conductor atom guides with circular cross sections and with subwavelength dimensions. The effects of the azimuthal components of the electromagnetic modes of such guides on the motion of atoms inside the guide were examined. The angular momentum features associated with the mode phase should involve a light-induced torque [21–23] and the consequent motion of atoms trapped in potential rings and guided through the structure was investigated.

Atom guiding can involve new aspects associated with

slow atoms; the quantum-mechanical nature of the vibrational states which, we expect, should play a role in the dynamics and the state of the dipole moment of a slow atom within the guide could have sufficient time to adjust to the mode polarization. These matters need to be discussed for cylindrical guides with circular cross section and their consequences for the dynamics of atoms in the circular guides are also needed in order to compare with the predictions assuming a fixed dipole orientation.

We envisage that the effect of the light torque due to a waveguide mode could be usefully exploited as, for example, in the focusing and stabilization of the guided beam that is simultaneously cooled by a one-dimensional molasses configuration involving a pair of counterpropagating waveguide modes. This laterally diffusion-free one-dimensional optical molasses configuration could make use of the light torque in conjunction with the axial friction force to generate samples of *in situ* cooled atoms and ions in the context of cylindrical guides. A related problem that can also be addressed is that of cylindrical atom guides with guide walls made of dielectrics characterized by dispersive dielectric functions which could also exhibit loss. A theory focusing on such features can, additionally, accommodate the first type of atom guide, namely, the evanescent mode guides which can now have the new feature of submicron dimensions. Work along these lines is now in progress and the results will be reported in due course.

- 
- [1] S. Al-Awfi and M. Babiker, *Phys. Rev. A* **58**, 2274 (1998).
  - [2] S. Al-Awfi and M. Babiker, *Phys. Rev. A* **58**, 4768 (1998).
  - [3] See, for example, J. M. Senior, *Optical Fiber Communications Principles and Practices*, 2nd ed. (Prentice Hall, Hemel Hempstead, 1992); J. Gower, *Optical Communications Systems*, 2nd ed. (Prentice Hall, Hemel Hempstead, 1995).
  - [4] M. A. Rippin and P. L. Knight, *J. Mod. Opt.* **47**, 807 (1996); K. Kakazu and Y. S. Kim, *Prog. Theor. Phys.* **96**, 883 (1996); H. Nha and W. Jhe, *Phys. Rev. A* **56**, 2213 (1997).
  - [5] M. A. Ol'Shanii, Y. B. Ovchinnikov, and V. S. Letokhov, *Opt. Commun.* **98**, 77 (1993).
  - [6] C. M. Savage, S. Marksteiner, and P. Zoller, in *Fundamentals of Quantum Optics III*, edited by F. Ehlotzky (Springer-Verlag, Berlin, 1993).
  - [7] S. Marksteiner, C. M. Savage, P. Zoller, and S. L. Rolston, *Phys. Rev. A* **50**, 2680 (1994).
  - [8] C. M. Savage, D. Gordon, and T. C. Ralph, *Phys. Rev. A* **52**, 3967 (1995); D. J. Harris and C. M. Savage, *ibid.* **51**, 3967 (1995).
  - [9] M. J. Renn, D. Montgomery, O. Vdovin, D. Z. Anderson, C. E. Wieman, and E. A. Cornell, *Phys. Rev. Lett.* **75**, 3253 (1995).
  - [10] M. J. Renn, E. A. Donley, E. A. Cornell, C. E. Wieman, and D. Anderson, *Phys. Rev. A* **53**, R648 (1996).
  - [11] H. Ito, K. Sakaki, T. Nakata, W. Jhe, and M. Ohtsu, *Opt. Commun.* **115**, 57 (1995).
  - [12] See, for example, N. S. Kapany and J. J. Burke, *Optical Waveguides* (Academic, London, 1972); D. Marcuse, *Theory of Dielectric Optical Wave Guides* (Academic, London, 1974).
  - [13] E. Hinds, *Adv. At., Mol., Opt. Phys.* **2**, 1 (1993).
  - [14] I. Bialynicki-Birula and Z. Bialynicka-Birula, *Phys. Rev. Lett.* **78**, 2539 (1997).
  - [15] M. P. Silverman, *Am. J. Phys.* **58**, 310 (1990).
  - [16] G. Nienhuis, J. P. Woerdman, and I. Kuscer, *Phys. Rev. A* **46**, 7079 (1992); J. P. Woerdman, G. Nienhuis, and I. Kuscer, *Opt. Commun.* **93**, 135 (1992).
  - [17] C. Courtial, K. Dholakia, A. Robertson, L. Allen, and M. J. Padgett, *Phys. Rev. Lett.* **80**, 3217 (1998).
  - [18] J. P. Dowling and J. Gea-Banaclache, *Adv. At., Mol., Opt. Phys.* **37**, 1 (1996).
  - [19] M. Kristensen, Mw. Beijesbergen, and J. P. Woerdman, *Opt. Commun.* **104**, 229 (1994).
  - [20] S. J. van Enk, *Quantum Opt.* **6**, 445 (1994); S. J. van Enk and G. Nienhuis, *J. Mod. Opt.* **41**, 963 (1994).
  - [21] L. Allen, M. Babiker, V. E. Lembessis, and W. K. Lai, *Phys. Rev. A* **54**, 4259 (1996).
  - [22] M. Babiker, V. E. Lembessis, W. K. Lai, and L. Allen, *Opt. Commun.* **123**, 524 (1996).
  - [23] M. Babiker, W. L. Power, and L. Allen, *Phys. Rev. Lett.* **73**, 1239 (1994).
  - [24] C. I. Suenik, M. G. Boshier, D. Cho, V. Sandoghdar, and E. A. Hinds, *Phys. Rev. Lett.* **70**, 560 (1993).